Magnetic and metallic state at intermediate Hubbard U coupling in multiorbital models for undoped iron pnictides

Rong Yu,[1,2] Kien T. Trinh,[3] Adriana Moreo,[1,2] Maria Daghofer,[1,2] José A. Riera,[4] Stephan Haas,[3] and Elbio Dagotto[1,2]
[1]*Department of Physics and Astronomy, The University of Tennessee, Knoxville, Tennessee 37996, USA*
[2]*Materials Science and Technology Division, Oak Ridge National Laboratory, Oak Ridge, Tennessee 32831, USA*
[3]*Department of Physics and Astronomy, University of Southern California, Los Angeles, California 90089, USA*
[4]*Instituto de Física Rosario, Consejo Nacional de Investigaciones Científicas y Técnicas, Universidad Nacional de Rosario, 2000 Rosario, Argentina*

(Received 15 December 2008; revised manuscript received 8 February 2009; published 13 March 2009)

Multiorbital Hubbard model Hamiltonians for the undoped parent compounds of the Fe-pnictide superconductors are investigated here using mean-field techniques. For a realistic four-orbital model, our results show the existence of an intermediate Hubbard U coupling regime where the mean-field ground state has a $(\pi,0)$ antiferromagnetic order, as in neutron-scattering experiments, while remaining metallic due to the phenomenon of band overlaps. The angle-resolved photoemission intensity and Fermi surface of this magnetic and metallic state are discussed. Other models are also investigated, including a two-orbital model where not only the mean-field technique can be used but also the exact diagonalization in small clusters and the variational cluster approximation in the bulk. The combined results of the three techniques point toward the existence of an intermediate-coupling magnetic and metallic state in the two-orbital model, similar to the intermediate-coupling mean-field state of the four-orbital model. We conclude that the state discussed here is compatible with the experimentally known properties of the undoped Fe pnictides.

DOI: 10.1103/PhysRevB.79.104510 PACS number(s): 71.10.Fd, 72.10.Di, 72.80.Ga, 79.60.−i

I. INTRODUCTION

The discovery of superconductivity in the Fe pnictides has opened an area of research that is attracting considerable attention.[1–8] In the early stages of these investigations, the layered structure of the Fe-pnictide superconductors,[1–8] the existence of a $(\pi,0)$ antiferromagnetic (AFM)-ordered state revealed by neutron scattering in the undoped limit,[9,10] and their large superconducting critical temperatures[1–8] motivated discussions on a possible close relation between these new Fe-based materials and the high-temperature cuprate superconductors. However, it was clear from the initial investigations that there were substantial differences as well, for example, the resistivity vs temperature curves of the parent compounds[1–8] do not show the characteristic Mott gapped behavior of, e.g., $LaCuO_4$. In fact LaOFeAs behaves as a bad metal or semiconductor[1–8] but not as an insulator. Moreover, the magnetic moment in the $(\pi,0)$ AFM-ordered state of LaOFeAs is much smaller than expected.[9,10] Although further neutron-scattering research has shown that the magnetic order parameters are larger in other Fe pnictides,[11] their values are still below those anticipated from band-structure calculations[12–16] or from the large Hubbard U limit of model Hamiltonians[17] (unless couplings are in a spin frustrated regime[18]). In summary, the parent compounds of the Fe superconductors behave in a manner different from the parent compounds of the Cu-oxide superconductors because the zero-temperature resistivity is finite and the magnetic order is weak. However, the pnictides are also different from BCS materials, where the normal state is a nonmagnetic metal with low resistivity. Then, the Fe superconductors appear to be in an *intermediate* regime of couplings, somewhere in between, e.g., MgB_2 and the Cu-oxide superconductors.[19,20] The "antiferromagnetic metallic" nature of LaOFeAs is clearly different from an AFM insulator or a nonmagnetic metal. Further confirming the need to focus on the intermediate-coupling regime for the Fe-pnictide parent compounds, a pseudogap has been observed[21–24] in the density of states (DOS) of the doped materials, which is different from the featureless DOS of a good metal or the gapped DOS of an insulator.[25]

Much of the current theoretical effort[17,18,26–47] has focused thus far on two well-defined limits. On one hand, band-structure calculations have reported the existence of Fermi pockets,[12–16] which were confirmed by photoemission experiments.[48–54] On the other hand, intuition on the physics of the model Hamiltonians is often gained by investigating the large U regime. Although results by some of us for a two-orbital model using numerical techniques have already shown that a small magnetic order can be accommodated at intermediate couplings,[17] this range of couplings is typically the most difficult to handle using computer simulations, and moreover, more bands are expected to be of relevance for a better quantitative description of the Fe pnictides.

In this paper, multiband Hubbard models are investigated using mean-field and numerical techniques. Our most important result is the discovery of an intermediate Hubbard U coupling regime where the ground state is an AFM metal. More specifically, for U larger than a critical value U_{c1} the $(\pi,0)$ AFM order develops with continuity from zero. In spite of a gap at particular momenta, the overall state remains metallic (there is a nonzero weight at the chemical potential in the DOS) due to the phenomenon of band overlaps. Further increasing the coupling to U_{c2}, a fully gapped insulator is stabilized. Thus, the intermediate regime $U_{c1} < U < U_{c2}$ is simultaneously (i) magnetic with a small order parameter and (ii) metallic. These properties are compatible with our current knowledge of the Fe-pnictide parent com-

pounds. Moreover, the DOS reveals the existence of a pseudogap in this regime. Since experiments addressing the pseudogap were mainly carried out in the doped case, our calculations then predict that a similar pseudogap should be observed in the undoped limit.

While these results are interesting, they were obtained using mean-field approximations. For the realistic case of four or five orbitals, it is difficult to obtain reliable numerical results to confirm the mean-field predictions. However, for the case of two orbitals, calculations can be carried out using simultaneously the mean-field technique, which also reveals an intermediate-coupling regime similar to that of the four- and five-orbital models, together with the exact diagonalization (ED) (Ref. 55) and variational cluster approximation (VCA) (Refs. 56 and 57) methods used before.[17] Below, it is reported that the results using these computational methods are compatible with those of the mean-field approximation, providing confidence that the mean-field method may have captured the essence of the problem. However, it is certainly desirable that future investigations confirm our main results.

For completeness, here some related previous literature is briefly mentioned. The band-overlap mechanism for an insulator-to-metal transition has been extensively studied before using band-structure calculations in a variety of contexts, such as TlCl and TlBr,[58] solid hydrogen,[59] and bromine under high pressure.[60] Closer to the present results, the existence of an intermediate Hubbard U regime with an AFM-metallic state was previously discussed by Duffy and Moreo[61] in the context of the high-temperature Cu-oxide superconductors and using the one-band Hubbard model, after introducing hopping terms t' and t'' between next-nearest-neighbor (NNN) sites. Density-functional methods were also used before to discuss AFM-metallic states and band-overlap insulator-metal transitions.[62,63] Within dynamical mean-field theory, an AFM-metallic state has also been discussed.[64] Experimentally, itinerant AFM states were found in the pyrite $NiS_{2-x}Se_x$,[65,66] in heavily doped manganites,[67] in ruthenates,[68] in organic conductors,[69,70] and in several other materials. An incommensurate spin density wave was also reported in metallic $V_{2-y}O_3$.[71] The results discussed in this paper establish an interesting connection between the Fe pnictides and the materials mentioned in this paragraph.

The organization of the paper is as follows. In Sec. II, results for a four-orbital model are presented. This includes a discussion of the model, the mean-field technique, and the results with emphasis on the intermediate-coupling state. The photoemission predictions for this state are discussed. In Sec. III, we show results for the two-orbital model using ED (Ref. 55) and VCA methods[56,57] in addition to mean-field approximations. Section IV contains our main conclusions.

II. RESULTS FOR A FOUR-ORBITAL MODEL

In this section, we will describe a possible minimal four-orbital model for the Fe-based superconductors. This model presents a Fermi surface (FS) similar to that obtained with band-structure calculations.

A. Four-orbital model

Previous studies have suggested that the Fe-As planes are the most important substructures of the full crystal that must be analyzed in order to reproduce the physical properties of the Fe pnictides close to the Fermi surface. We consequently focus on these Fe-As planes in the present study. The effective Fe-Fe hopping Hamiltonian, using As as a bridge, can be obtained within the framework of the Slater-Koster (SK) formalism.[72] By this procedure, here we will construct a minimal model defined on a Fe square lattice, consisting of the four Fe d orbitals xz, yz, xy, and x^2-y^2. It is assumed that the $d_{3z^2-r^2}$ orbital lies at a substantially lower energy and is thus always filled with two electrons.[12–16] While the SK procedure is not as quantitatively accurate as a full band-structure calculation, it can still provide the proper model Hamiltonian because it correctly takes into account the geometry of the system and illustrates which orbitals are connected to one another at different lattice sites. Thus, our procedure here will be to use the SK method to construct the formal model, and then obtain the actual numerical values of the hopping parameters via comparison with band-structure calculations.

The Hamiltonian $H=H_0+H_{\text{int}}$ includes two parts: the hopping term H_0 and the interaction term H_{int}. The hopping term in real space reads

$$H_0 = \sum_{\mathbf{i},\mathbf{j}} \sum_{\mu,\nu} \sum_{\sigma} (T^{\mu,\nu}_{\mathbf{i},\mathbf{j}} d^{\dagger}_{\mathbf{i},\mu,\sigma} d_{\mathbf{j},\nu,\sigma} + \text{H.c.}), \tag{1}$$

where $d^{\dagger}_{\mathbf{i},\mu,\sigma}$ creates an electron at site $\mathbf{i}$ with spin σ on the μth orbital ($\mu=1,2,3,4$ stands for the xz, yz, xy, and x^2-y^2 orbitals, respectively). Here, hoppings at nearest neighbors (NNs) and also at NNNs along the plaquette diagonals were considered. The hopping tensor $T^{\mu,\nu}_{\mathbf{i},\mathbf{j}}$ has a complicated real-space structure that will not be reproduced here. H_0 has a simpler form when transformed to momentum space,

$$H_0 = \sum_{\mathbf{k}} \sum_{\mu,\nu} \sum_{\sigma} T^{\mu,\nu}(\mathbf{k}) d^{\dagger}_{\mathbf{k},\mu,\sigma} d_{\mathbf{k},\nu,\sigma}, \tag{2}$$

with

$$T^{11} = -2t_2 \cos k'_x - 2t_1 \cos k'_y - 4t_3 \cos k'_x \cos k'_y, \tag{3}$$

$$T^{22} = -2t_1 \cos k'_x - 2t_2 \cos k'_y - 4t_3 \cos k'_x \cos k'_y, \tag{4}$$

$$T^{12} = -4t_4 \sin k'_x \sin k'_y, \tag{5}$$

$$T^{33} = -2t_5[\cos(k'_x+\pi) + \cos(k'_y+\pi)] - 4t_6 \cos(k'_x+\pi)\cos(k'_y+\pi) + \Delta_{xy}, \tag{6}$$

$$T^{13} = -4it_7 \sin k'_x + 8it_8 \sin k'_x \cos k'_y, \tag{7}$$

$$T^{23} = -4it_7 \sin k'_y + 8it_8 \sin k'_y \cos k'_x, \tag{8}$$

$$T^{44} = -2t_{17}[\cos(k'_x+\pi) + \cos(k'_y+\pi)] - 4t_9 \cos(k'_x+\pi)\cos(k'_y+\pi) + \Delta_{x^2-y^2}, \tag{9}$$

$$T^{14} = -4it_{10} \sin k'_y, \tag{10}$$

$$T^{24} = 4it_{10} \sin k'_x, \tag{11}$$

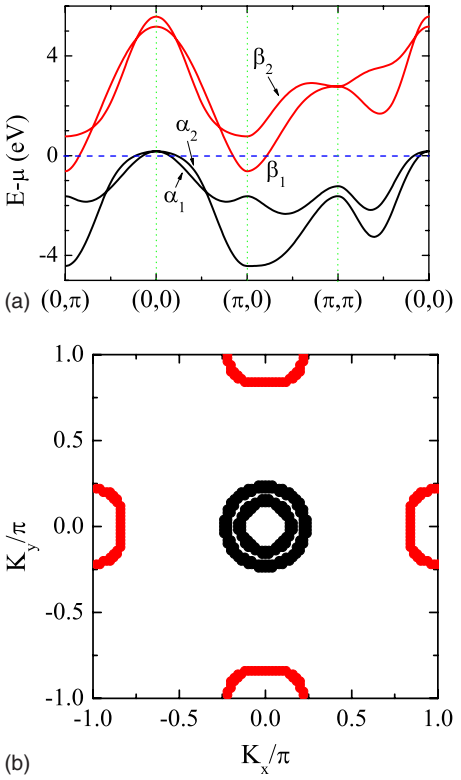

FIG. 1. (Color online) (a) Band structure corresponding to the four-orbital tight-binding Hamiltonian Eq. (2) using the LDA-fitted values of the hopping parameters provided in Table I. The Fermi surface is formed by two holelike bands (α_1, α_2) and one electronlike band (β_1). The chemical potential is at 0. (b) The topology of the corresponding Fermi surface.

$$T^{34} = 0. \tag{12}$$

Equation (2) represents a matrix in the basis $\{d^{\dagger}_{\mathbf{k},\mu,\sigma}\}$ where $\mathbf{k}=\mathbf{k}'$ if $\mu=1$ or 2 and $\mathbf{k}=\mathbf{k}'+\mathbf{Q}$ if $\mu=3$ or 4 with $-\pi<k_x,k_y\leq\pi$, $\mathbf{k}'$ is defined in the reduced Brillouin zone (BZ) corresponding to the two-Fe unit cell, and $\mathbf{Q}=(\pi,\pi)$. In other words, the above expressions couple states with momentum $\mathbf{k}'$ for orbitals xz and yz to states with momentum $\mathbf{k}'+\mathbf{Q}$ for orbitals xy and x^2-y^2. The momentum $\mathbf{Q}$ appears after considering the staggered location of the As atoms above and below the plane defined by the Fe atoms. As already mentioned, the mathematical form of this model arises directly from the Slater-Koster considerations. This problem is equivalent to an eight-orbital model with a Hamiltonian expanded in the basis $\{d^{\dagger}_{\mathbf{k}',\mu,\sigma}, d^{\dagger}_{\mathbf{k}'+\mathbf{Q},\mu,\sigma}\}$. As a result, the eight-orbital band structure and Fermi surface (Fig. 2) are obtained by "folding" the results in the equivalent four-orbital problem (Fig. 1).

The actual values of the hopping parameters could in principle be obtained from the overlap integrals in the SK formalism.[72,73] However, to properly reproduce the Fermi surface obtained in the local-density approximation (LDA) (Refs. 12–16), it is better to fit the values of those hoppings. The parameters used, as well as the on-site energies Δ_μ for the xy and x^2-y^2 orbitals, are listed in Table I. The on-site energy term is given by $\Sigma_{\mathbf{i},\mu}\Delta_\mu n^{\mu}_{\mathbf{i}}$ (standard notation) and it is part of the tight-binding Hamiltonian.

TABLE I. Fitted hopping parameters and on-site energies for the four-orbital model used in Sec. II A (in eV units).

Δ_{xy}	−0.600	$\Delta_{x^2-y^2}$	−2.000
t_1	0.500	t_2	0.150
t_3	−0.175	t_4	−0.200
t_5	0.800	t_6	−0.450
t_7	0.460	t_8	0.005
t_9	−0.800	t_{10}	−0.400
t_{17}	0.900		

In Figs. 1 and 2, we show the band structure and the corresponding Fermi surface for the four-orbital tight-binding Hamiltonian in Eq. (2) using Table I. Since we assume that the $3z^2-r^2$ orbital is always doubly occupied, the chemical potential in the undoped case is determined by locating $n=4$ electrons per site in the four bands considered here. As shown in Fig. 1(b), two hole pockets centered at (0,0) (arising from the α_1 and α_2 bands) and four pieces of two electron pockets centered at $(0,\pi)$ and $(\pi,0)$ (from the β_1 band) are obtained. The shape of the Fermi surface qualitatively reproduces the band-structure LDA calculations[12–16] after a 45° rotation about the center of the first Brillouin zone (FBZ), as presented in Fig. 2(b), due to the rotation from the Fe-Fe axis to the Fe-As axis.

To study the relation between the orbital hybridization and the Fermi-surface topology, the projected weight of each

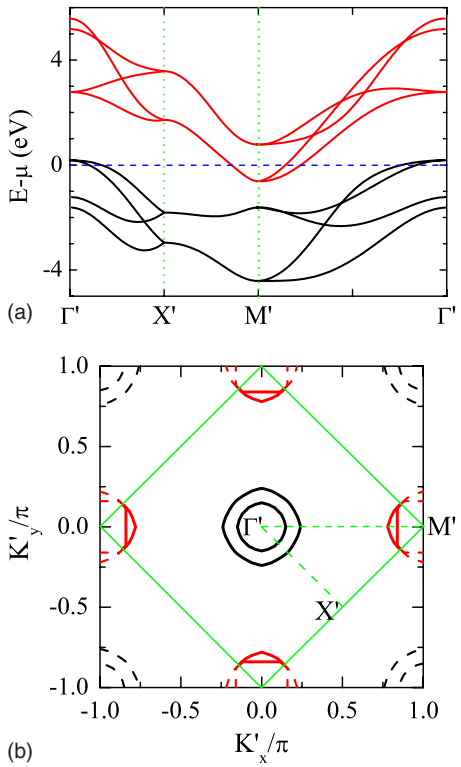

FIG. 2. (Color online) (a) Band structure of the eight-orbital problem in the reduced BZ obtained by folding the results presented in Fig. 1(a). (b) Fermi surface of the eight-orbital problem obtained by folding the FS obtained in Fig. 1(b). The FS in the first (second) BZ are indicated by continuous (dashed) lines.

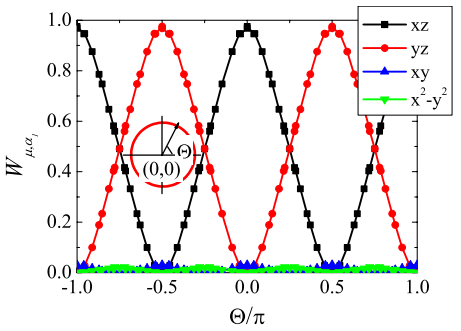

FIG. 3. (Color online) The projected orbital weight $W_{\mu,\lambda}$ of states at the Fermi surface. Shown, as example, are results for the outer hole pocket centered at (0,0). The definition of Θ is given in the inset.

orbital at both the hole and electron pockets were calculated. These weights are defined via the eigenvectors of H_0: $W_{\mu,\lambda}(\mathbf{k})=\frac{1}{2}\Sigma_\sigma|U_{\mathbf{k},\mu,\sigma;\lambda}|^2$, where λ denotes the band index $(\alpha_1,\alpha_2,\beta_1,\beta_2)$ and μ refers to the four d orbitals. The matrix $U_{\mathbf{k},\mu,\sigma;\lambda}$ diagonalizes the system [see Eq. (18) below]. An example of the angle-resolved weights in momentum space is shown in Fig. 3. The two hole pockets centered at (0,0) mostly arise from the xz and yz orbitals, compatible with LDA (Refs. 12–16) and with much simpler descriptions based only on two orbitals.[17,36] The electron pocket centered at $(\pi,0)$ $[(0,\pi)]$ arises mainly from the hybridization of the xz $[yz]$ and xy orbitals (not shown). These results are also qualitatively consistent with those from the first-principles calculations.[16] However, there are some quantitative discrepancies that lead us to believe that probably longer range than the NNN plaquette-diagonal hoppings are needed to fully reproduce the LDA results including orbital weights. Nevertheless, the discussion below on the metallic magnetic phase at intermediate couplings is robust, and we believe that it will survive when more complex multiorbital models are used in the future.

Note that the eigenenergies (band dispersion) along the $(0,0)\rightarrow(\pi,0)$ and $(0,0)\rightarrow(0,\pi)$ directions are symmetric about (0,0), but the eigenvectors $(W_{\mu,\lambda})$ show a large anisotropy. For instance, at the Fermi level the α_1 band is almost xz-like along the $(0,0)\rightarrow(\pi,0)$ direction but almost yz-like along the $(0,0)\rightarrow(0,\pi)$ direction. Below, it will be discussed how this anisotropy affects the mean-field results for the interacting system.

Let us now consider the interaction term,[17] which reads

$$H_{\text{int}}=U\sum_{\mathbf{i},\mu}n_{\mathbf{i},\mu,\uparrow}n_{\mathbf{i},\mu,\downarrow}+\left(U'-\frac{J}{2}\right)\sum_{\mathbf{i},\mu<\nu}n_{\mathbf{i},\mu}n_{\mathbf{i},\nu}-2J\sum_{\mathbf{i},\mu<\nu}\mathbf{S}_{\mathbf{i},\mu}\cdot\mathbf{S}_{\mathbf{i},\nu},\quad(13)$$

where $\mathbf{S}_{\mathbf{i},\mu}$ $(n_{\mathbf{i},\mu})$ is the spin (charge density) of orbital μ at site $\mathbf{i}$ and $n_{\mathbf{i},\mu}=n_{\mathbf{i},\mu,\uparrow}+n_{\mathbf{i},\mu,\downarrow}$. The first term is a Hubbard repulsion for the electrons in the same orbital. The second term describes an on-site interorbital repulsion, where the standard relation $U'=U-J/2$ caused by rotational invariance is used.[74] The last term in Eq. (13) is a Hund term with a ferromagnetic coupling J. A complete description would also require a pair-hopping interaction similar to the last term of Eq. (24), where the interaction term for the two-orbital model is shown. But ED was used to test its impact in the case of two orbitals, and it was not found to be important. Consequently, it was neglected in the mean-field treatment.

B. Mean-field approach

To study the ground-state properties of the system, we apply a mean-field approximation to the model Hamiltonian described by Eqs. (1)–(13). We follow here the simple standard assumption of considering only the mean-field values for the diagonal operators,[75]

$$\langle d^\dagger_{\mathbf{i},\mu,\sigma}d_{\mathbf{j},\nu,\sigma'}\rangle=\left[n_\mu+\frac{\sigma}{2}\cos(\mathbf{q}\cdot\mathbf{r}_\mathbf{i})m_\mu\right]\delta_{\mathbf{ij}}\delta_{\mu\nu}\delta_{\sigma\sigma'},\quad(14)$$

where $\mathbf{q}$ is the ordering vector of the possible magnetic order. n_μ and m_μ are mean-field parameters describing the charge density and magnetization of the orbital μ, and the rest of the notation is standard. Applying Eq. (14) to H_{int}, the mean-field Hamiltonian in momentum space can be written as

$$H_{\text{MF}}=H_0+C+\sum_{\mathbf{k},\mu,\sigma}\epsilon_\mu d^\dagger_{\mathbf{k},\mu,\sigma}d_{\mathbf{k},\mu,\sigma}+\sum_{\mathbf{k},\mu,\sigma}\eta_{\mu,\sigma}(d^\dagger_{\mathbf{k},\mu,\sigma}d_{\mathbf{k}+\mathbf{q},\mu,\sigma}+d^\dagger_{\mathbf{k}+\mathbf{q},\mu,\sigma}d_{\mathbf{k},\mu,\sigma}),\quad(15)$$

where $\mathbf{k}$ runs over the extended FBZ, H_0 is the hopping term in Eq. (2),

$$C=-NU\sum_\mu\left(n_\mu^2-\frac{1}{4}m_\mu^2\right)-N(2U'-J)\sum_{\mu\neq\nu}n_\mu n_\nu+\frac{NJ}{4}\sum_{\mu\neq\nu}m_\mu m_\nu$$

is a constant, N is the lattice size, and we used the definitions

$$\epsilon_\mu=Un_\mu+(2U'-J)\sum_{\nu\neq\mu}n_\nu,\quad(16)$$

$$\eta_{\mu,\sigma}=-\frac{\sigma}{2}\left(Um_\mu+J\sum_{\nu\neq\mu}m_\nu\right).\quad(17)$$

The above mean-field Hamiltonian can be numerically solved for a fixed set of mean-field parameters using standard library subroutines. The parameters n_μ and m_μ are obtained in a self-consistent manner by minimizing the energy. In practice an initial guess for n_μ and m_μ serves as a set of input parameters for a given value of the couplings U and J. The mean-field Hamiltonian is then diagonalized and n_μ and m_μ are re-evaluated using Eq. (14). This procedure is iterated until both n_μ and m_μ have converged. During the iterative procedure $\Sigma_\mu n_\mu=4$ was enforced at each step such that the total charge density is a constant. Note that in the mean-field approximation an electron with momentum $\mathbf{k}$ is coupled to an electron with momentum $\mathbf{k}+\mathbf{q}$, where $\mathbf{q}$ is the vector associated with the magnetic ordering. Then, the Hamiltonian

in Eq. (15) is solved only in the magnetic reduced Brillouin zone with only half of the size of the unfolded FBZ.

The numerical solution of the mean-field Hamiltonian immediately allows for the evaluation of the band structure, the density of states (DOS), and the magnetization ($M=\Sigma_\mu m_\mu$) at the ordering wave vector $\mathbf{q}$. Moreover, we can also calculate the photoemission spectral function. Assuming that the mean-field Hamiltonian Eq. (15) is diagonalized by the unitary transformation,

$$d_{\mathbf{k},\mu,\sigma} = \sum_{\lambda} U_{\mathbf{k},\mu,\sigma;\lambda}\gamma_\lambda, \tag{18}$$

$$H_{\mathrm{MF}} = \sum_{\lambda} \rho_\lambda \gamma_\lambda^\dagger \gamma_\lambda, \tag{19}$$

then the spectral function is given by

$$A(\mathbf{k},\omega) = \sum_{\lambda} \sum_{\mu,\nu,\sigma} U_{\mathbf{k},\mu,\sigma;\lambda} U^\dagger_{\lambda;\mathbf{k},\nu,\sigma} \delta(\omega - \rho_\lambda). \tag{20}$$

In practice $\delta(\omega-\rho_\lambda)$ was here substituted by $\frac{1}{\pi}\frac{\varepsilon}{\varepsilon^2+(\omega-\rho_\lambda)^2}$ with a broadening $\varepsilon=0.05$ eV.

C. Mean-field results

In this section, the mean-field results for the four-orbital model previously described are presented. Experimentally, a (bad) metallic phase with antiferromagnetic order was observed in the undoped compound LaOFeAs.[9,10] It is then important to investigate in the mean-field approximation the properties of such a state. Here we show the numerical results for the mean-field approximation defined on a 100×100 square lattice.

1. Magnetic order

To study in more detail the magnetic ordered state, the ordering wave vector $\mathbf{q}$ is assumed here to be $(0,\pi)$ in the mean-field approximation. In Fig. 4(a), the evolution of the magnetization vs U, at $J=U/4$, is shown. At a critical value $U_{c1}=1.90$ eV, the $(0,\pi)$ order[76] starts to grow continuously from zero. This $(0,\pi)$ magnetization increases slowly until it reaches $U_{c2}=3.75$ eV, where it changes discontinuously, showing the characteristic of a first-order transition (see discussion for the origin of this transition later in this section). Note that for $U\leq U_{c2}$, the magnetization for the $(0,\pi)$ state is smaller than 1.0 (with a normalization such that the maximum possible value is 4.0), indicating that there is an intermediate U regime that can accommodate the rather weak $(0,\pi)$ magnetic order found in the neutron-scattering experiments.[9,10] In Fig. 4(b), magnetization curves for the same state at various values of J are presented. Two transitions for all J/U ratios studied are observed, similarly as for $J=U/4$ in (a).

2. Band structure and Fermi surfaces

Let us analyze in more detail the $(\pi,0)$ AFM-ordered state. Since varying J/U does not significantly alter the results, the value $J=U/4$ is adopted in the rest of the analysis. In Figs. 5–7 the band structures and Fermi surfaces of this

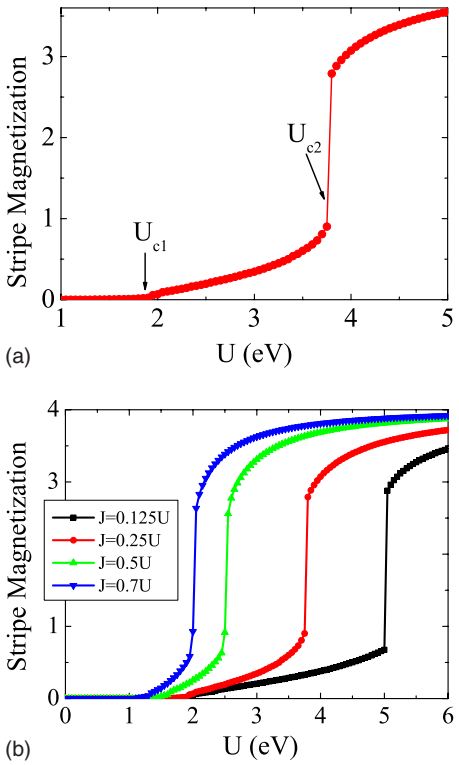

FIG. 4. (Color online) (a) The mean-field evolution with U of the magnetization of the state ordered at wave vector $(0,\pi)$ with $J=U/4$. Shown are the two critical values: one where the magnetization becomes nonzero and a second one where a discontinuous behavior is concomitant with a metal-to-insulator transition, as described in text. (b) The same magnetization curve as in (a) but for several values of J/U. The magnetization shown in (a) and (b) is normalized such that the maximum value is 4, corresponding to four spin polarized electrons, one per orbital, at each site.

state at several values of U are extracted from the calculated mean-field photoemission spectral-function data. Both the band structure and the Fermi surface at the critical point $U_{c1}=1.90$ eV are, of course, identical to those at $U=0$ in Fig. 1. This noninteracting electronic description of the system changes gradually upon the establishment of the $(0,\pi)$ AFM order. As discussed in more detail below, gaps open at particular momenta, while other bands crossing the Fermi surface do not open a gap. Thus, this is a metallic regime with magnetic order. Finally, at the magnetization discontinuity a full gap develops.

3. Bands of magnetic origin in the $(0,\pi)$ antiferromagnetic state

Due to the off-diagonal term in Eq. (15), an electron with momentum $\mathbf{k}$ is coupled to another with momentum $\mathbf{k}+\mathbf{q}$ if their orbital characters are the *same*. This generally leads to avoided level crossings and opens a gap proportional to the magnetization. If the hole and electron Fermi surfaces can be connected by the vector $\mathbf{q}$, then a magnetic state with spin ordering at $\mathbf{q}$ is stabilized over the nonmagnetic state due to the Fermi-surface nesting effect. The magnetic state gains energy via the opening of a gap near the Fermi level. This magnetically ordered state significantly changes the band

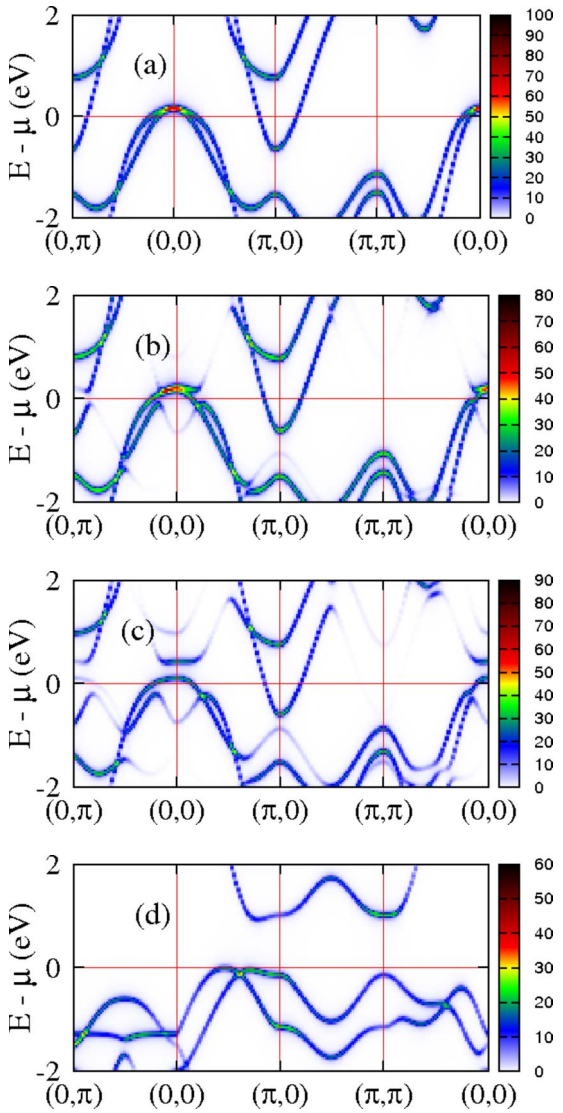

FIG. 5. (Color online) Mean-field photoemission band structure of the $(0,\pi)$ AFM state in the energy window [−2 eV, 2 eV] at $U=1.90$ eV, $U=2.50$ eV, $U=3.20$ eV, and $U=4.00$ eV, from top to bottom, with $J=U/4$. The first U is at the first transition and still has the shape of the noninteracting limit. The second two values of U are in the intermediate-coupling regime, and the presence of states at energy 0 (location of the chemical potential) indicate a metallic state. The last coupling, $U=4.00$ eV, is above the second critical point, and thus already in the gapped regime. In the two intermediate couplings, 2.50 and 3.20 eV, weak bands not present in the noninteracting limit (top panel) are revealed. These are the bands caused by the $(0,\pi)$ AFM order, which should be observable in photoemission experiments.

structure of the noninteracting case. As shown in Figs. 5(b) and 5(c), gaps open in this magnetically ordered phase, which is consistent with the depletion of the spectral weight close to the Fermi level found using the dynamical mean-field approximation.[77] More interestingly, the magnetic order gives rise to the emergence of new bands of magnetic origin, sometimes called the "shadow bands," also shown in Figs. 5(b) and 5(c), and with more detail for a special case in Fig. 6. Similar issues were discussed in the context of high-

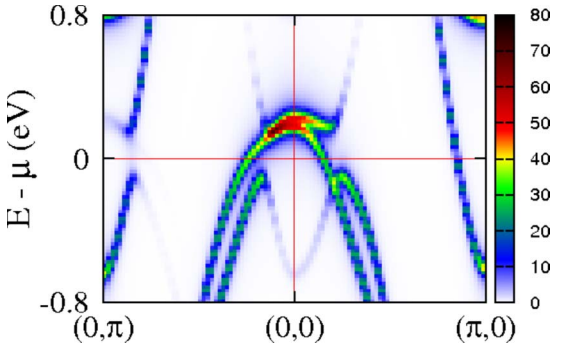

FIG. 6. (Color online) Mean-field photoemission band structure of the $(0,\pi)$ AFM state in the energy window [−0.8 eV, 0.8 eV] at $U=2.50$ eV. Bands caused by magnetic order that are not present in the nonmagnetic case $U=0.0$ are shown here in more detail than in Fig. 5.

temperature superconductors, where the existence of bands caused by the staggered magnetic order was extensively studied before.[78] In fact, experiments for undoped cuprates revealed a photoemission spectral function in excellent agreement with theoretical expectations,[79] i.e., containing the predicted bands generated by the magnetic order. Thus, it is to be expected that the $(0,\pi)$ AFM order of the Fe pnictides should also produce magnetically induced bands in the undoped limit and even in the doped case if the magnetic correlation length remains large enough.

4. First-order transition at U_{c2}

Regarding the second transition at U_{c2}, the qualitative reason for its presence lies in the incompatibility of the intermediate-coupling metallic state with the large U limit. The mechanism of nesting that causes the special features of the intermediate U state previously discussed, including the survival of portions of the Fermi surface, will lead to an energy that eventually cannot compete with a fully gapped state at large U at the electronic density considered here; thus a transition must eventually occur.

But why is the second transition discontinuous? In Fig. 5 the coupling between the hole pockets and the electron pocket at $(0,\pi)$ leads to the distortion of the Fermi surface in the $(0,\pi)$ AFM state. Such a coupling between states with a specific orbital symmetry and momentum also accounts for the metallic nature of the $(0,\pi)$ AFM state; the electron pocket at $(\pi,0)$ is almost undistorted for $U<U_{c2}$. However, when U is approaching the second critical value U_{c2}, the peak at (π,π) with occupied states in the α_1 band becomes energetically closer to the Fermi level (its energy is increasing with U). If the Fermi-surface nesting effect could be neglected at U_{c2}, then a smooth behavior would be observed since the charges could transfer continuously from the peak at (π,π), after crossing the Fermi level, to the peak at (0,0). However, note that the valley of the β_1 band at $(\pi,0)$ and the peak of the α_1 band at (π,π) have both a partial xy symmetry. Moreover, they are connected by the vector $\mathbf{q}=(0,\pi)$. Thus, it will be expected that a gap close to the Fermi level will open to minimize the energy. At U_{c2}, the system gains

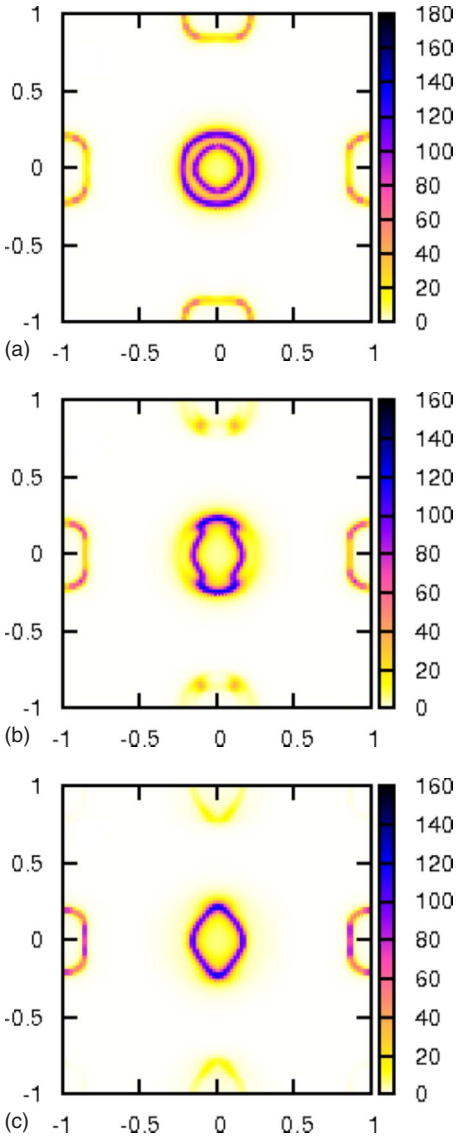

FIG. 7. (Color online) Mean-field photoemission Fermi surfaces in the $(0,\pi)$ AFM-ordered state at $U=1.90$ eV, $U=2.50$ eV, and $U=3.20$ eV from top to bottom. The results are obtained via $A(\mathbf{k},\omega)$ using a window of 20 meV centered at the Fermi energy. Shown are results obtained from an equal weight average of data using $A(\mathbf{k},\omega)$ and $A(\mathbf{p},\omega)$, where $\mathbf{k}=(k_x,k_y)$ and $\mathbf{p}=(k_x,-k_y)$. By this procedure the results are properly symmetrized under rotations in the nonmagnetic phase. The anisotropy of the results in the $(0,\pi)$ ordered intermediate U region does appear because the spin order breaks rotational invariance.

maximal energy by opening a finite gap at both $(\pi,0)$ and (π,π), and lowering the energy of the α bands at (0,0) such that they become fully occupied. This leads to discontinuous changes in the population of the individual orbitals, producing discontinuous changes in the orbital magnetizations, and concomitantly, a finite gap. Since in the real undoped Fe-pnictide materials the full-gap regime is not realistic, then we can proceed with the rest of the analysis below without further consideration of this discontinuity in the magnetization.

5. Anisotropic Fermi surface in the undoped parent compound

The appearance of the $(0,\pi)$ magnetism with magnetically induced bands leads to an *anisotropic* distortion of the Fermi surface in the magnetically ordered state. For instance, consider the $\mathbf{q}=(0,\pi)$ mean-field state. To predict the pattern of gaps in this state, the information previously discussed in, e.g., Fig. 3, is important. Through the projected weights, it was observed that the β_1 electron pocket centered at $(0,\pi)$ has mainly $yz+xy$ symmetry, while the $(\pi,0)$ electron pocket has mainly $xz+xy$. A dominance of the yz symmetry is found in the α_1 hole pocket along the $(0,0)\rightarrow(0,\pm\pi)$ directions and in the α_2 hole pocket along the $(0,0)\rightarrow(\pm\pi,0)$ directions. Then, for the magnetic state with $\mathbf{q}=(0,\pi)$, a gap should open in the $(0,0)\rightarrow(0,\pm\pi)$ directions for the α_1 (inner hole pocket) band and for the electron pocket at $(0,\pi)$, but the α_2 (outer hole pocket) band remains gapless. In addition, a gap opens in the $(0,0)\rightarrow(\pm\pi,0)$ directions for the α_2 band, but both the inner hole pocket and the $(\pi,0)$ electron pocket remain gapless. These results are indeed observed numerically as shown in Figs. 5(b) and 5(c).

Due to these anisotropic gaps, the Fermi surfaces of the α bands change their topology from two pockets [Fig. 7(a)] to four arcs that are very close to one another, as shown in Fig. 7(b). In between the arcs, there is actually a nonzero but weak intensity at the location of the original hole pockets. For LaOFeAs, since a weak $(0,\pi)$ AFM order has been observed, the Fermi surface is expected to have a similar shape as that shown in Fig. 7(b). However, topology of the Fermi surface in this state is sensitive to the value of the coupling U; further increasing this coupling the four arcs merge into a single pocket [Fig. 7(c)]. Then, angle-resolved photoemission spectroscopy (ARPES) experiments can provide valuable information about the exact shape of the Fermi surface, and thus, the interaction strength.

Besides the anisotropic gaps near the Fermi level, gaps far from the Fermi level also exist [see, for instance, Fig. 5(b)]. This cannot occur in a one-band model because the opening of these gaps would not provide any energy gain. However, such gaps are possible in more complex multiorbital models; since the off-diagonal term in Eq. (15) depends on the magnetization that is contributed by each orbital, once the magnetic state is stabilized by the opening of a gap near the Fermi level, the off-diagonal term becomes nonzero even for the bands far from the Fermi level.

A rather surprising result is that the intensities of the spectral function of the two α pockets display an anisotropy even in the nonmagnetic phase (not shown). This is puzzling since from Fig. 3, it can be observed that $\Sigma_\mu W_{\mu,\lambda}(\mathbf{k})=1$ for any $\mathbf{k}$. Naively, this would lead to an isotropic $A(\mathbf{k},\omega)$. However, from Eq. (20), $A(\mathbf{k},\omega)=\Sigma_\lambda \delta(\omega-\rho_\lambda)W'_\lambda(\mathbf{k})$, where

$$W'_\lambda(\mathbf{k})=\sum_\sigma \left|\sum_\mu U_{\mathbf{k},\mu,\sigma,\lambda}\right|^2. \tag{21}$$

Here, note that an anisotropy could arise from the interference between different orbitals. To observe this more explicitly, W'_λ for the two α hole pockets at $U=0$ is shown in Fig. 8. These functions are not constant but oscillate between 0

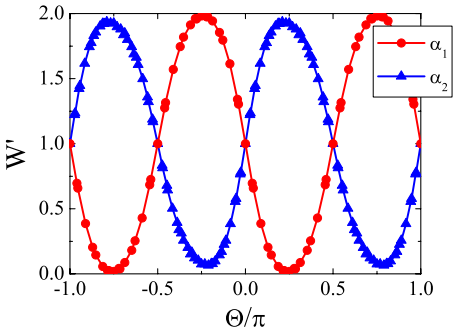

FIG. 8. (Color online) The angular resolved weight W' at $U=0$ obtained using Eq. (21) for the two α holelike pockets. The definition of Θ is the same as in Fig. 3.

and 2. From Fig. 8, it is observed that for the α_1 band W' reaches its maximum at, e.g., $-\pi/4$, corresponding to the $(0,0)\rightarrow(-\pi,\pi)$ direction, while for the α_2 band, the maximum of W' is at, e.g., $\pi/4$, i.e., in the $(0,0)\rightarrow(\pi,\pi)$ direction. Such an anisotropy in $A(\mathbf{k},\omega)$ is not a consequence of the mean-field approximation but is related to the multiband nature of the model itself. Interestingly, such an anisotropy in the topology of the Fermi surface in the $A(\mathbf{k},\omega)$ data may account for the anisotropic features of the hole pocket in the recent ARPES experiment on LaOFeP,[80] where a long-ranged $(0,\pi)$ AFM order is absent.[81] However, in Fig. 7 this problem is avoided by a symmetrization procedure (see caption of Fig. 7) that restores rotational invariance to the nonmagnetic state. Thus, the anisotropy of the important intermediate U regime fully originates in the lack of rotational invariance of the antiferromagnetic state with a wave vector $(0,\pi)$ or $(\pi,0)$.

6. Metallic magnetically ordered phase at intermediate couplings and existence of a pseudogap

As already remarked, Fig. 5 indicates that for moderate U the magnetically ordered system is still gapless, i.e., it is in a metallic phase with a finite Fermi surface due to the phenomenon of "band overlapping" described in Sec. I. This intermediate state is also revealed via the evolution of the DOS in Fig. 9. As displayed in Fig. 9(a), a pseudogap in the DOS near the chemical potential exists in the regime $U_{c1}<U<U_{c2}$. If the availability of states at the Fermi level is assumed to be directly related with transport properties, a DOS pseudogap suggests bad-metallic characteristics in the intermediate U regime. Hence, the finding of a pseudogap in the intermediate U regime is consistent with several theoretical studies that have suggested that the parent iron pnictide is a bad metal.[18,77,82,83] The pseudogap turns into a hard gap at $U>U_{c2}$, where the system becomes an insulator. In Fig. 9(b) the value of the DOS at the chemical potential vs U is plotted. Two transitions can be easily identified. For $U<U_{c1}$, $N(\mu)$ is a constant. It decreases continuously for $U>U_{c1}$, indicating a second-order transition from the paramagnetic metallic phase to the metallic phase with antiferromagnetic order. At $U>U_{c2}$, it drops abruptly to a small value, corresponding to the formation of a full gap in the insulating

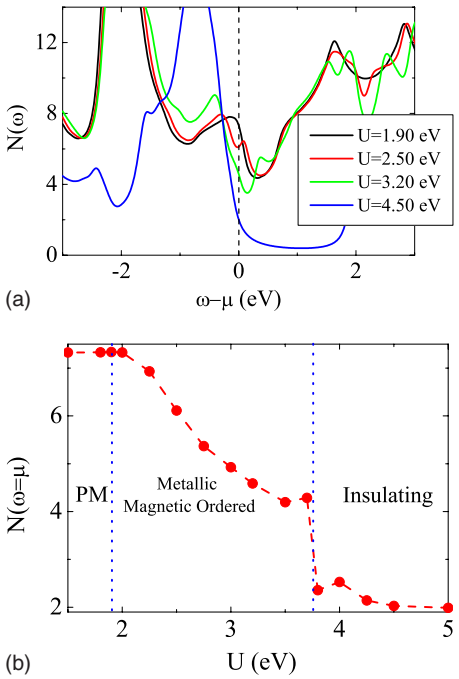

FIG. 9. (Color online) (a) Density of states at various values of U showing the development of a pseudogap at the chemical potential in the $(0,\pi)$ AFM-ordered state. (b) The evolution of $N(\omega)$, the DOS at the chemical potential, indicates three well-separated regions. The nonzero values of $N(\omega=\mu)$ in the insulating phase at $U>U_{c2}$ arise from the finite broadening of the raw DOS numerical data.

phase (the finite DOS at large U is simply caused by the artificial broadening of delta functions to plot results).

7. Stability of the $(\pi,0)$ antiferromagnetic phase

Consider now the stability of the antiferromagnetic-ordered state by analyzing two possible magnetically ordered states: one with $\mathbf{q}=(0,\pi)$ and another one with (π,π). The U dependence of the magnetization and the energy difference between these two states are presented in Fig. 10. The (π,π) order appears at $U\approx 2.5$ eV, which is higher than the U_{c1} for the $(0,\pi)$ state. However, with increasing U, the (π,π) staggered magnetization increases much faster than for the $(0,\pi)$

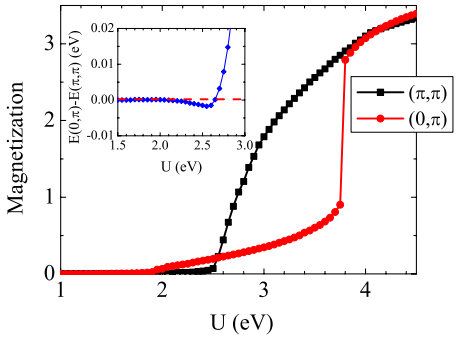

FIG. 10. (Color online) Main panel: the evolution of the magnetization with U for $\mathbf{q}=(0,\pi)$ and (π,π). Inset: energy difference between the two states of the main panel.

AFM state. As shown in the inset of Fig. 10, the (π,π) state becomes more stable than the $(0,\pi)$ state for $U \geq 2.65$ eV. We have analyzed several other sets of hopping parameters and ratios J/U, and the results are qualitatively the same; the $(0,\pi)$ states are stable but in a narrow region of couplings.

Hence, in our model the $(0,\pi)$ AFM-ordered ground state becomes unstable to another AFM state with $\mathbf{q}=(\pi,\pi)$ at $U \geq 2.65$ eV through a first-order transition. This is not too surprising considering the values of the hopping parameters; the NN and NNN hoppings are similar in magnitude. Thus, there is a competition between different spin tendencies, as it occurs at intermediate couplings in Heisenberg spin systems with NN and NNN terms. However, the neutron-scattering experiments show that the ground state of several undoped Fe pnictides presents *only* the $(\pi,0)$ AFM order (which in our model is degenerate with the $(0,\pi)$ AFM state considered in this section). To understand the predominance of this state over the (π,π) AFM state, note that it has been argued that the emergence of the $(\pi,0)$ AFM state is closely related to a structural phase transition[9,10] from space group $P4/nmm$ to $P112/n$. The lattice distortion at the transition breaks the fourfold rotational symmetry and lifts the degeneracy of the xz and yz orbitals. Thus, according to recent calculations that incorporate the lattice distortion, the system prefers the $(\pi,0)$ state over the (π,π) state.[35] Since the effects of lattice distortions are not included in our model, then the (π,π) spin-ordered state apparently strongly competes with the $(0,\pi)$-$(\pi,0)$ spin states but this is misleading and caused by the absence of lattice energetic considerations.

This discussion leads us to believe that simply analyzing the $(0,\pi)$ AFM state found in the mean-field approximation should be sufficient to understand some of the electronic properties of the real system. However, it is remarkable that even in the competing (π,π) ordered state there are also two magnetically ordered phases: a metallic phase for moderate U values and an insulating phase with a finite gap at larger U values (see Fig. 11). This qualitatively agrees with the previous analysis for the $(0,\pi)$ AFM-ordered phase. This suggests that the existence of a metallic magnetically ordered phase at moderate U is an intrinsic property of the multiorbital Hubbard model, treated in the mean-field approximation, which is robust varying the interactions, as discussed in more detail in Sec. II C 8.

8. Mean-field results for other models with several active orbitals

We have applied the mean-field technique to several other multiorbital models such as a five-orbital model,[26] another four-orbital model,[30] and an effective three-orbital model including the xz, yz, and xy orbitals.[34] For all these multiband models a Coulombic interaction term similar to Eq. (13) has been used. A robust conclusion of our mean-field analysis is that a transition from a paramagnetic metal to a metallic $(0,\pi)$ AFM-ordered state is found in all the models considered here.

Let us discuss the results for the five-orbital model.[26] This model does not give precisely the correct Fermi-surface topology in the undoped case since it contains a pocket at (π,π). This problem can be fixed by slightly modifying the

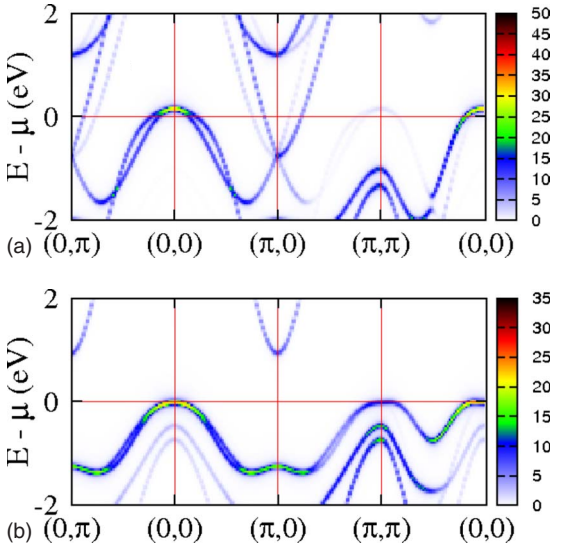

FIG. 11. (Color online) Mean-field band structures of the spin-ordered (π,π) state in the energy window [−2 eV, 2 eV]. The upper panel is obtained at $U=2.75$ eV where the band overlap indicates a metallic state even if the order parameter is nonzero. The lower panel is at $U=4.50$ eV where the gap is fully developed.

electronic concentration to, e.g., $n=6.2$. However, in our study we will consider $n=6.0$ for consistency with the rest of the analysis. Within the mean-field approximation, the magnetization at $n=6.0$ is shown in Fig. 12. In this case there is a broad region of metallicity, and the second critical Hubbard coupling (also indicated) does not involve a discontinuity. The Fermi surface in the inset shows pockets at (0,0), $(\pi,0)$, $(0,\pi)$, and (π,π). We conclude that a variety of multiorbital models show similar features as the four-orbital model analyzed before, particularly regarding an intermediate metallic magnetic phase.

III. RESULTS FOR THE TWO-ORBITAL MODEL

The complexity of four- and five-orbital Hamiltonians leads to very large Hilbert spaces even for small clusters, and as a consequence, it is not possible to compare the mean-field results against exact diagonalization (ED) (Ref. 55) or

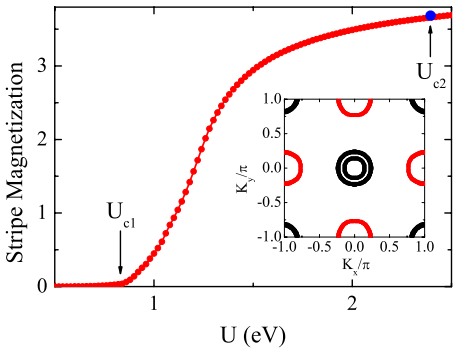

FIG. 12. (Color online) Main panel: the evolution of the magnetization for the state with $\mathbf{q}=(0,\pi)$ in a five-orbital model (Ref. 26) at electron filling $n=6.0$. Inset: the Fermi surface at $U=0$.

variational cluster approach (VCA) (Refs. 56 and 57) results. For this reason the two-orbital model, which was recently studied with ED and VCA methods,[17] is revisited here to assess the validity of the mean-field approximation. Our conclusion is that all three techniques lead to similar results for the two-orbital model, lending support to our claim for the existence of an intermediate-coupling metallic and magnetic state.

The two-orbital model has been widely analyzed in recent literature and its derivation and other properties will not be repeated here. It is given by

$$H_{2o} = H_K + H_{\rm int}, \tag{22}$$

where the kinetic energy H_K in real space is[17,36]

$$\begin{aligned} H_K = &- t_1 \sum_{\mathbf{i},\sigma} (d^\dagger_{\mathbf{i},x,\sigma} d_{\mathbf{i}+\hat{y},x,\sigma} + d^\dagger_{\mathbf{i},y,\sigma} d_{\mathbf{i}+\hat{x},y,\sigma} + \text{H.c.}) \\ &- t_2 \sum_{\mathbf{i},\sigma} (d^\dagger_{\mathbf{i},x,\sigma} d_{\mathbf{i}+\hat{x},x,\sigma} + d^\dagger_{\mathbf{i},y,\sigma} d_{\mathbf{i}+\hat{y},y,\sigma} + \text{H.c.}) \\ &- t_3 \sum_{\mathbf{i},\hat{\mu},\hat{\nu},\sigma} (d^\dagger_{\mathbf{i},x,\sigma} d_{\mathbf{i}+\hat{\mu}+\hat{\nu},x,\sigma} + d^\dagger_{\mathbf{i},y,\sigma} d_{\mathbf{i}+\hat{\mu}+\hat{\nu},y,\sigma} + \text{H.c.}) \\ &+ t_4 \sum_{\mathbf{i},\sigma} (d^\dagger_{\mathbf{i},x,\sigma} d_{\mathbf{i}+\hat{x}+\hat{y},y,\sigma} + d^\dagger_{\mathbf{i},y,\sigma} d_{\mathbf{i}+\hat{x}+\hat{y},x,\sigma} + \text{H.c.}) \\ &- t_4 \sum_{\mathbf{i},\sigma} (d^\dagger_{\mathbf{i},x,\sigma} d_{\mathbf{i}+\hat{x}-\hat{y},y,\sigma} + d^\dagger_{\mathbf{i},y,\sigma} d_{\mathbf{i}+\hat{x}-\hat{y},x,\sigma} + \text{H.c.}) \\ &- \mu \sum_{\mathbf{i}} (n_{\mathbf{i},x} + n_{\mathbf{i},y}). \end{aligned} \tag{23}$$

The form of H_K in momentum space was provided in Refs. 17 and 36 and is given by Eqs. (3)–(5) of the four-orbital model. The Coulomb interaction terms are

$$\begin{aligned} H_{\rm int} = &U \sum_{\mathbf{i},\alpha} n_{\mathbf{i},\alpha,\uparrow} n_{\mathbf{i},\alpha,\downarrow} + (U' - J/2) \sum_{\mathbf{i}} n_{\mathbf{i},x} n_{\mathbf{i},y} - 2J \sum_{\mathbf{i}} \mathbf{S}_{\mathbf{i},x} \cdot \mathbf{S}_{\mathbf{i},y} \\ &+ J \sum_{\mathbf{i}} (d^\dagger_{\mathbf{i},x,\uparrow} d^\dagger_{\mathbf{i},x,\downarrow} d_{\mathbf{i},y,\downarrow} d_{\mathbf{i},y,\uparrow} + \text{H.c.}), \end{aligned} \tag{24}$$

where the notation is the same as for the case of the four-orbital model but with $\alpha = x, y$ here denoting the orbitals xz and yz. The index $\hat{\mu}$ is a unit vector linking NN sites and takes the values $\hat{x}$ or $\hat{y}$. μ is the chemical potential. As for the case of four orbitals, the relation $U' = U - 2J$ originating in rotational invariance[74] was used. In the last term in Eq. (24), the same rotational invariance also establishes that the pair-hopping coupling J' must be equal to J. As before, the hoppings are determined from the orbital integral overlaps within the SK formalism or from LDA band dispersion fittings.[17,36] Most of the properties of this two-orbital model are formally similar to those of the four-orbital model, and as a consequence, several details of the analysis of Sec. II do not need to be repeated here.

A. Mean-field approximation

Following the same procedure used for the four-orbital model, here we consider only the mean-field values that are diagonal with respect to the Fe site, orbital, and spin labels such that

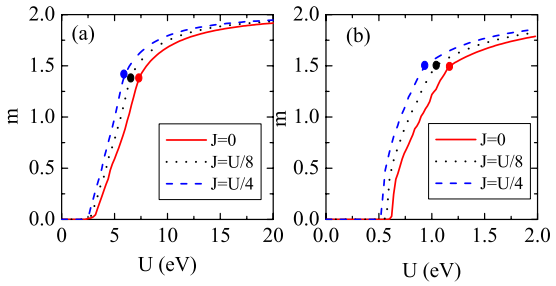

FIG. 13. (Color online) Two-orbital model mean-field calculated $(\pi, 0)$ ordered magnetization m vs U. Panel (a) is for the LDA-fitted hoppings (Ref. 36), while panel (b) is for the SK hoppings (Ref. 17). The solid red line is for $J=0$. With a blue dashed line the results at $J=U/4$ are indicated. The dotted black line denotes results for $J=U/8$. The large dot in each curve indicates the value of m at U_{c2} where the metal-to-insulator transition occurs (see text). Note the absence of a first-order transition at U_{c2} as in the four-orbital model.

$$\langle d^\dagger_{\mathbf{l},\alpha,\sigma} d_{\mathbf{l}',\alpha',\sigma'} \rangle = \left[n_\alpha + \frac{\sigma}{2} \cos(\mathbf{q} \cdot \mathbf{r}_\mathbf{l}) m_\alpha \right] \delta_{\mathbf{l}\mathbf{l}'} \delta_{\alpha\alpha'} \delta_{\sigma\sigma'}. \tag{25}$$

After introducing Eq. (25) to decouple the four-fermion interactions in Eq. (24), and then transforming into momentum space, we obtain

$$\begin{aligned} H^{\rm MF}_{\rm int} = &- UN \sum_\alpha \left(n_\alpha^2 - \frac{1}{4} m_\alpha^2 \right) - 4 \left(U' - \frac{J}{2} \right) N n_x n_y \\ &+ \frac{JN m_x m_y}{2} + \sum_{\mathbf{k},\sigma} \left[U n_x + 2 \left(U' - \frac{J}{2} \right) n_y \right] n_{\mathbf{k}x\sigma} \\ &+ \sum_{\mathbf{k},\sigma} \left[U n_y + 2 \left(U' - \frac{J}{2} \right) n_x \right] n_{\mathbf{k}y\sigma} \\ &- \frac{1}{4} \sum_{\mathbf{k}\sigma} (U m_x + J m_y)(d^\dagger_{\mathbf{k}x\sigma} d_{\mathbf{k}+\mathbf{q}x\sigma} + d^\dagger_{\mathbf{k}+\mathbf{q}x\sigma} d_{\mathbf{k}x\sigma}) \\ &- \frac{1}{4} \sum_{\mathbf{k}\sigma} (U m_y + J m_x)(d^\dagger_{\mathbf{k}y\sigma} d_{\mathbf{k}+\mathbf{q}y\sigma} + d^\dagger_{\mathbf{k}+\mathbf{q}y\sigma} d_{\mathbf{k}y\sigma}). \end{aligned} \tag{26}$$

The four mean-field parameters n_x, n_y, m_x, and m_y are determined in the usual way by minimizing the energy and by requesting that the system be half filled. The half-filling condition determines that $n_x = n_y = 0.5$ while the values of m_x and m_y are a function of U and J. We have observed that varying U and for fixed J, m_α becomes nonzero at a critical value $U = U_{c1}$ where a gap opens separating the "valence" and "conduction" bands at particular momenta, but overall, there is still an overlap in the energy of some bands and the chemical potential crosses both of them. Thus, the system has developed magnetic order but it is still a metal. However, the bands no longer overlap when $U > U_{c2}$, and thus, a metal-insulator transition occurs. These results are similar to those obtained using more orbitals in the model.

In Fig. 13, the $(\pi, 0)$ ordered magnetization $m = m_x + m_y$ vs

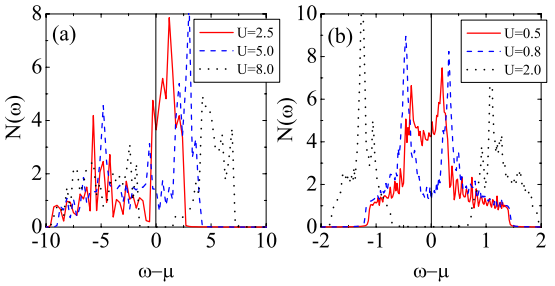

FIG. 14. (Color online) Two-orbital model mean-field calculated density of states (a) for the LDA-fitted hoppings (Ref. 36) and (b) for the SK hoppings (Ref. 17). Panel (a): the solid red line is for $U=2.5$, blue dashed line is for $U=5.0$, and dotted black line is for $U=8.0$. Panel (b): solid red is for $U=0.5$, blue dashed is for $U=0.8$, and dotted black is for $U=2.0$. $J=U/4$ is used in both panels.

U is shown for $J=0$, $U/4$, and $U/8$. Panel (a) contains the results for the LDA-fitted hoppings[36] while panel (b) is for the SK hoppings[17] with $pd\sigma=-0.2$. The critical coupling U_{c1} is the value of U where m becomes different from zero. There is a second critical coupling U_{c2} that is obtained by monitoring the density of states, and it separates a metallic from an insulating regime. For completeness, this second coupling is indicated with a full circle for each case. In panel (b), the shape of the curves is the same for the three values of J investigated, and the actual value of U_{c1} mildly depends on J.

The mean-field density of states (DOS) $N(\omega)$ is presented in Fig. 14 for some values of U and $J=U/4$, and the two sets of hoppings considered here. The solid curve in both panels shows results for $U<U_{c1}$. In this case the system is metallic. The dashed curve displays the DOS for a value of U in between the two critical points. Although the DOS varies continuously as U increases, it is clear that this regime is qualitatively different. A deep pseudogap has developed at the chemical potential. The system is still metallic in this regime, although likely with "bad metal" characteristics. Finally, the dotted curve shows the DOS for $U>U_{c2}$. In this case, there is a gap at the chemical potential and the system has become insulating. Interestingly, the transition at U_{c2} is not first order for the two-orbital model, in contrast to the case with four orbitals.

B. Mean-field results for the bands and Fermi surface

The mean-field band structure obtained by solving the mean-field self-consistent equations is shown along high-symmetry directions in the Brillouin zone in Fig. 15. The panels on the left (right) column correspond to LDA-fitted (SK) hoppings. The top row shows the band dispersion for $U<U_{c1}$. The corresponding Fermi surface (FS) in the extended and reduced Brillouin zones (BZs) are shown in Figs. 16(a) and 16(c), and they agree with previous discussions for the two-orbital model.[17]

The second row of panels in Fig. 15 shows the band dispersion in the interesting regime $U_{c1}<U<U_{c2}$. It can be observed that gaps have opened along, e.g., the direction $(0,0)$-$(0,\pi)$ but not along other high-symmetry directions.

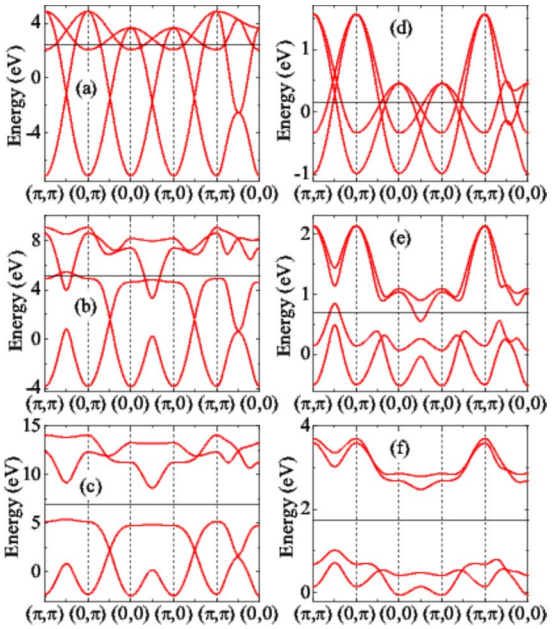

FIG. 15. (Color online) Two-orbital model mean-field band structure along high-symmetry directions in the extended FBZ. The panels on the left column show results for the LDA-fitted hoppings (Ref. 36), while results on the right are for the SK hoppings (Ref. 17). (a) $U=2.5$, (b) $U=5.0$, (c) $U=8.0$, (d) $U=0.5$, (e) $U=0.8$, and (f) $U=2.0$. In all cases, $J=U/4$ and the magnetic order wave vector is $(\pi,0)$.

The partial gaps remove portions of the original FS and produce the $A(\mathbf{k},\omega)$ disconnected features (arcs) at Γ shown in panel (b) of Fig. 16. Note that in Fig. 7(b), the results for the four-orbital model also contained arcs but they appeared in a more symmetric manner, namely, with four arcs surrounding

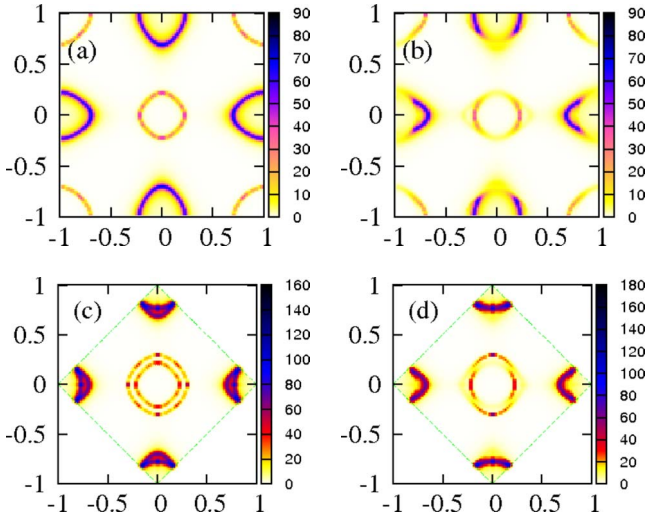

FIG. 16. (Color online) Mean-field photoemission Fermi surface for the LDA-fitted hoppings (Ref. 36) in the unfolded FBZ for (a) $U=1$ and (b) $U=3$, and in the folded FBZ for (c) $U=1$ and (d) $U=3$. The ratio $J=U/4$ was used, and the magnetic order wave vector is $(\pi,0)$. These results were obtained via $A(\mathbf{k},\omega)$ using the same symmetrization procedure and energy window centered at the Fermi energy as in Fig. 7.

the Γ point. Two of those arcs were located in the inner hole pocket and two in the outer hole pocket, while in Fig. 16(b) there are only two arcs around the Γ point. However, as often remarked in the context of the two-orbital model, to compare with either experiments or results of models with more orbitals, it is crucial to fold the results since by this mechanism the hole pocket at M becomes the outer hole pocket at Γ. Following this procedure, in Fig. 16(d) the folded results are shown and now there are *four arcs* around the Γ point, in good agreement with the results of the four-orbital model. We conclude that in the interesting intermediate-coupling regime, both models give similar results upon folding of the extended Brillouin zone.

The last row of panels in Fig. 15 shows the band dispersion for $U > U_{c2}$. Now the upper and lower bands no longer overlap. The gap is complete and there is no FS. The system has become an insulator, as can be seen in the DOS shown in Fig. 14.

The intensity of the features determining the Fermi surface should be calculated using the spectral function $A(\mathbf{k},\omega)$. Figure 15 only shows the eigenvalues of the mean-field study without incorporating the photoemission intensity of each state. It is only when the strength of the coupling U becomes very large that the spectral weights for all the bands will be equal. Otherwise, some of the bands will produce strong FS while others will produce only weak magnetically induced "shadow" features that are hard to observe, as already shown in Fig. 16. To better visualize the bands induced by magnetic order, in Fig. 17 the mean-field spectral function $A(\mathbf{k},\omega)$ is presented along the high-symmetry directions in the BZ for the two-orbital model with the SK parameters.[17] For $U < U_{c1}$, panel (a), the spectral weight resembles the noninteracting band structure, i.e., there is negligible spectral weight in the magnetically induced bands. For $U_{c1} < U < U_{c2}$, panel (b), the bands become distorted and the bands of magnetic origin develop particularly at the locations in which a gap opens. There are other bands still crossing the Fermi energy; thus the system is metallic. Finally for $U > U_{c2}$, panel (c), the gap is complete and the magnetic bands are well developed, i.e., four peaks can be observed in $A(\mathbf{k},\omega)$ for almost all values of $\mathbf{k}$. Figure 18 shows the results for the LDA-fitted hoppings[36] at $J=U/4$; here a similar qualitative discussion applies. Other values of J such as $J=0$ and $J=U/8$ (not shown) were also considered, and the results are qualitatively the same.

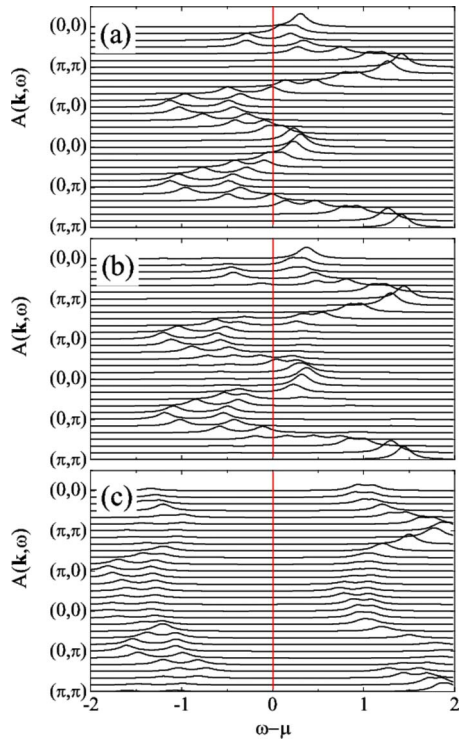

FIG. 17. (Color online) Two-orbital model mean-field spectral function along high-symmetry directions in the extended FBZ using SK hoppings (Ref. 17). (a) $U=0.5$, (b) $U=0.8$, and (c) $U=2.0$. The Hund coupling is fixed to $J=U/4$ and the magnetic order wave vector is $(\pi,0)$.

C. Exact diagonalization results

To analyze the qualitative reliability of the mean-field results, we have performed ED calculations on finite clusters. In our previous effort,[17] it was discussed that due to the rapid growth of the Hilbert space with the number of sites N, the largest cluster where the two-orbital model can be exactly diagonalized has only $N=8$ sites. It is a tilted $\sqrt{8}\times\sqrt{8}$ cluster, and when periodic boundary conditions are implemented, the available values of the momenta are $\mathbf{k}=(0,0)$, $(\pm\pi/2,\pm\pi/2)$, $(0,\pi)$, $(\pi,0)$, and (π,π). This limited set of momenta is not well suited to analyze band dispersions in the BZ, and the use of "twisted" boundary conditions (TBCs) (see below) for the eight-site cluster would require a computational effort that is too high. However, via the study of spin correlations it has been observed that the $(\pi,0)$ AFM order characteristic of this model is also apparent in the even smaller 2×2 cluster. For this very small system, the limited number of available momenta can be enlarged by implementing TBCs, namely, requesting that $d(N_i+1)=e^{i\phi}d(1)$ where N_i is the number of sites along the $i=x$ or y direction in the square cluster and ϕ is an arbitrary phase. With these TBCs the values of momenta allowed are now $k_i=\frac{2\pi n_i+\phi}{N_i}$ with n_i ranging from 0 to N_i-1. Thus, we can calculate the spectral functions for a variety of values of $\mathbf{k}$ using this TBC approach applied to the 2×2 cluster. While the very small size is still a serious limitation, note that there are simply no other procedures available to contrast the mean-field results against exact results at intermediate couplings. Our goal using this limited size cluster is merely to analyze if mean-field conclusions stand against exact results.

In Fig. 19, the spectral function $A(\mathbf{k},\omega)$ is presented along the main diagonal of the extended BZ for different values of U and with $J=U/4$. These data have to be compared with the mean-field prediction shown in Fig. 18. We present the results for $U=0$ for comparison and to demonstrate that the correct dispersion is obtained in spite of the fact that the cluster is so small. The finite values of U have been chosen to be in the magnetic-metallic region ($U=2.5$ and 5.0) and in the insulating region ($U=8$) according to the mean-field results. The main point of this figure is to report the development of bands induced by magnetic order with increasing U.

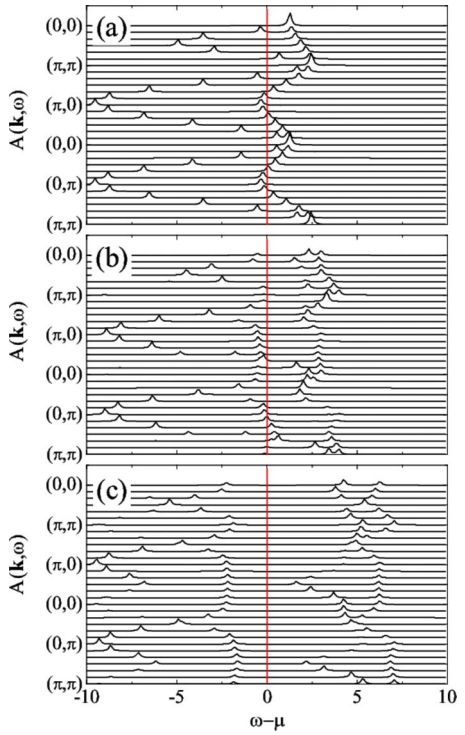

FIG. 18. (Color online) Two-orbital model mean-field spectral function along high-symmetry directions in the extended FBZ for the LDA-fitted hoppings (Ref. 36). The couplings used are (a) $U=2.5$, (b) $U=5$, and (c) $U=8$. In all cases $J=U/4$, and the magnetic order wave vector is $(\pi,0)$.

A representative momentum for these magnetically induced bands is highlighted with an arrow in the figure. With increasing U, the magnetic bands smoothly develop [concomitant with the development of $(\pi,0)$ AFM order at short distances, as will be shown later] and at least along the main-diagonal direction in the extended FBZ that should occur simultaneously with the opening of a gap. Thus, our first conclusion is that the extra weak features in the one-particle

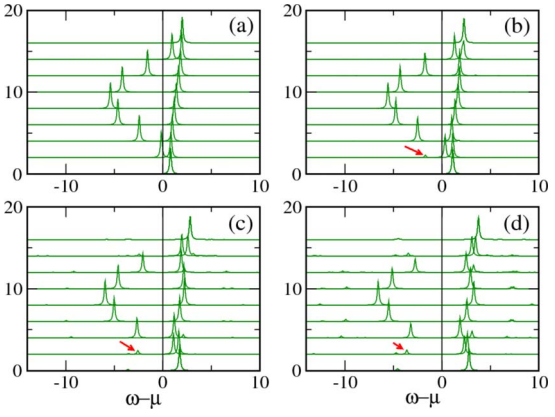

FIG. 19. (Color online) Two-orbital model spectral function along the (0,0) to (π,π) direction in the extended FBZ for the LDA-fitted hoppings (Ref. 36). (a) is for $U=0.0$, (b) is for $U=2.5$, (c) is for $U=5.0$, and (d) is for $U=8.0$. The Hund coupling is $J=U/4$. The method is ED and the lattice is 2×2 with TBC. The arrows indicate the magnetic bands discussed in text.

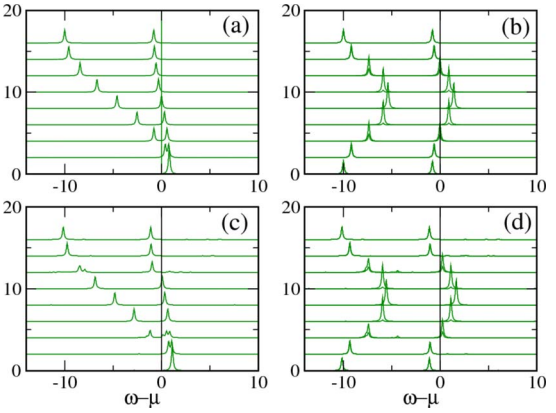

FIG. 20. (Color online) Two-orbital model spectral function along the (0,0) to $(\pi,0)$ and $(\pi,0)$ to $(0,\pi)$ directions in the extended FBZ for the LDA-fitted hoppings (Ref. 36). (a) and (b) are for $U=0$, while (c) and (d) are for $U=2.5$. The Hund coupling is $J=U/4$. The method is ED and the lattice is 2×2 with TBC. This figure shows that the results barely change between the two values of U, suggesting the survival of a metallic state at nonzero U.

spectral function predicted by mean field due to the magnetic order do appear in the ED results. At large U there is no doubt that a substantial gap is observed, as in the mean-field approach. We also performed calculations with other values of J such as $J=0$ and $J=U/8$ (not shown), and the conclusions are qualitatively the same as for $J=U/4$. Qualitatively similar conclusions were reached using the SK hoppings.[17]

Let us analyze now other directions in momentum space. In Fig. 20, the (0,0) to $(\pi,0)$ and $(\pi,0)$ to $(0,\pi)$ directions are investigated at $U=0$ and 2.5. The results indicate negligible changes along these directions by turning on U; the system appears to remain metallic. However, as shown below, the NN $(\pi,0)$ AFM order in this small cluster is already robust at $U=2.5$. Thus, these results are compatible with the concept of a state simultaneously metallic and magnetically ordered. Moreover, by monitoring the opening of the complete gap we found that the metal-insulator transition occurs at a value of U_{c2}, in good agreement with the mean-field predictions. The existence of a U_{c1} is a more complicated issue but it can be inferred from the development of the magnetic bands in $A(\mathbf{k},\omega)$ which also occurs in a range of U consistent with the mean field.

In Fig. 21 we present the magnetic structure factor S for $\mathbf{k}=(0,\pi)$ which is the value of the momentum for which it has a maximum [degenerate with $(\pi,0)$ for this small cluster]; panel (a) shows results for the SK hoppings[17] while panel (b) is for the LDA-fitted hoppings.[36] To reduce the finite-size effects, results for the $N=8$ cluster are presented, although the results in the 2×2 cluster are qualitatively similar. For large U, the monotonic increase in S with U agrees with the mean-field results. At small and intermediate U, the $(\pi,0)$ correlations are robust, and for these small clusters this is equivalent to long-range order. But the apparent lack of a gap at $U=2.5$ along particular directions in momentum space (discussed before) leads us to believe that the ED results are compatible with a metallic and magnetic phase at intermediate U.

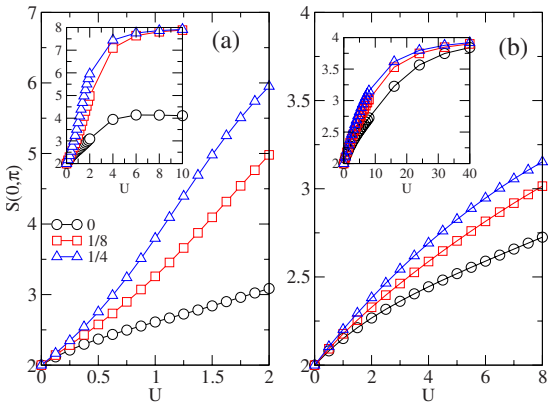

FIG. 21. (Color online) The magnetic structure factor at $\mathbf{k}=(0,\pi)$ vs U calculated by ED of an eight-site cluster for the values of J indicated. (a) is for the SK hoppings (Ref. 17) and (b) is for the LDA-fitted hoppings (Ref. 36). The insets show the results in a more extended range of U.

D. VCA results

In this final section, numerical results for the spectral functions and the density of states obtained with the VCA technique[56,57] are presented. This method embeds the ED solution of a small 2×2 cluster into a very large system of a size comparable to the 100×100 momentum points used in the mean field, and thus interpolates between the results obtained independently by the ED and mean-field approaches. The VCA results discussed here are for the SK parameters.[17] Figure 22 shows the VCA density of states. The behavior with increasing U is remarkably similar to that obtained in our mean-field calculations presented in Fig. 14(b). Metallic, pseudogap, and insulating regimes can be clearly observed.

The results for $A(\mathbf{k},\omega)$ calculated with VCA are shown in Fig. 23. Once again, a remarkable quantitative agreement with the mean-field results of Fig. 17 is found.

IV. CONCLUSIONS

In this investigation, the mean-field technique was applied to multiorbital Hubbard models for the Fe pnictides. Varying

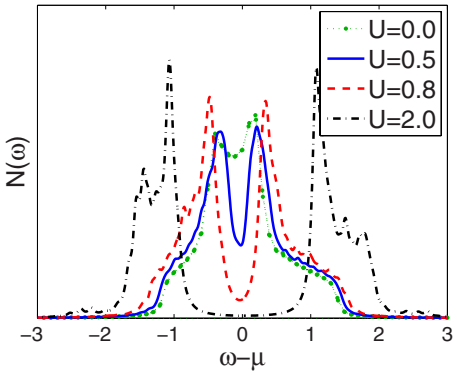

FIG. 22. (Color online) VCA-calculated density of states for different values of U in the metallic (good metal and pseudogap) and insulating regimes with the SK hopping parameters using $pd\pi/pd\sigma=-0.2$ and $J=U/4$.

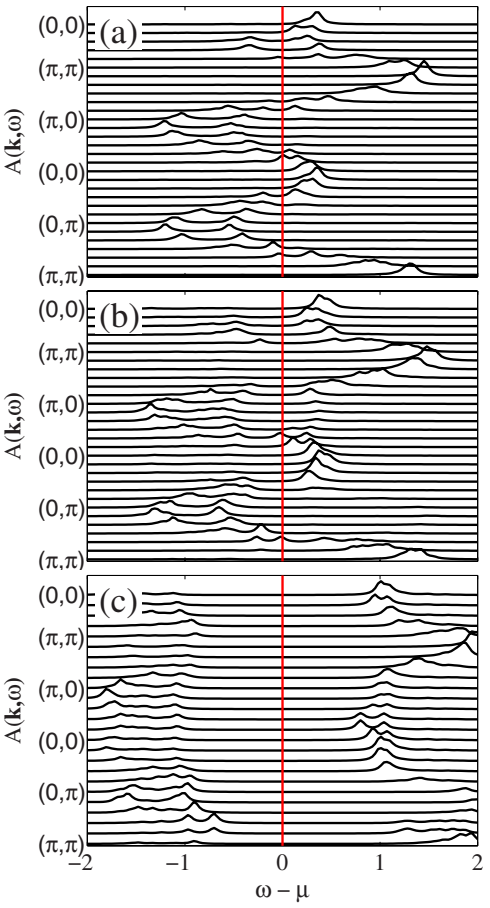

FIG. 23. (Color online) VCA-calculated spectral functions along high-symmetry directions in the BZ for the SK hopping parameters with $pd\pi/pd\sigma=-0.2$, $J=U/4$, and wave vector $(\pi,0)$. (a) $U=0.5$; (b) $U=0.8$; (c) $U=2.0$.

U, three regions were observed. At small coupling, the results are as in the noninteracting limit. In the other extreme of very large U, the ground state has a robust gap and the $(\pi,0)$ AFM order parameter is large. The main result of our effort is the presence of an intermediate U coupling regime where a $(\pi,0)$ AFM order is shown to coexist with a metallic ground state due to band overlaps. This state has similar characteristics as the parent compounds of the Fe-pnictide superconductors. From the DOS, our effort predicts that a pseudogap should be observed in the undoped parent compounds, similarly as already found in the doped case. Although further theoretical work is still needed to firmly establish the existence of this interesting intermediate-coupling regime, for the case of two orbitals our conclusions were tested using the ED and VCA methods, and the results are compatible with mean field.

The analysis of the intermediate U regime allowed us to predict the results for angle-resolved photoemission experiments. Interesting anisotropies manifested as arcs at the Fermi surface. New bands of magnetic origin were also discussed. The two- and four-orbital models lead to similar results in this context. Future work will address the optical properties of the intermediate-coupling regime and the superconducting state that may arise from its doping.

ACKNOWLEDGMENTS

This work was mainly supported by the NSF under Grant No. DMR-0706020 and the Division of Materials Science and Engineering, U.S. DOE under contract with UT-Battelle, LLC. Computation for part of the work described in this paper was supported by the University of Southern California Center for High Performance Computing and Communications. S.H. and K.T. acknowledge financial support from the National Science Foundation under Grant No. DMR-0804914 and the Department of Energy under Grant No. DE-FG02-05ER46240.

[1] Y. Kamihara, T. Watanabe, M. Hirano, and H. Hosono, J. Am. Chem. Soc. **130**, 3296 (2008).
[2] G. F. Chen, Z. Li, G. Li, J. Zhou, D. Wu, J. Dong, W. Z. Hu, P. Zheng, Z. J. Chen, H. Q. Yuan, J. Singleton, J. L. Luo, and N. L. Wang, Phys. Rev. Lett. **101**, 057007 (2008).
[3] G. F. Chen, Z. Li, D. Wu, G. Li, W. Z. Hu, J. Dong, P. Zheng, J. L. Luo, and N. L. Wang, Phys. Rev. Lett. **100**, 247002 (2008).
[4] H.-H. Wen, G. Mu, L. Fang, H. Yang, and X. Zhu, EPL **82**, 17009 (2008).
[5] X. H. Chen, T. Wu, G. Wu, R. H. Liu, H. Chen, and D. F. Fang, Nature (London) **453**, 761 (2008).
[6] Z.-A. Ren, W. Lu, J. Yang, W. Yi, X.-L. Shen, Z.-C. Li, G.-C. Che, X.-L. Dong, L.-L. Sun, F. Zhou, and Z.-X. Zhao, Chin. Phys. Lett. **25**, 2215 (2008).
[7] Z.-A. Ren, J. Yang, W. Lu, W. Yi, G.-C. Che, X.-L. Dong, L.-L. Sun, and Z.-X. Zhao, Mater. Res. Innovations **12**, 105 (2008).
[8] Z.-A. Ren, G.-C. Che, X.-L. Dong, J. Yang, W. Lu, W. Yi, X.-L. Shen, Z.-C. Li, L.-L. Sun, F. Zhou, and Z.-X. Zhao, EPL **83**, 17002 (2008).
[9] C. de la Cruz, Q. Huang, J. W. Lynn, Jiying Li, W. Ratcliff II, J. L. Zarestky, H. A. Mook, G. F. Chen, J. L. Luo, N. L. Wang, and P. Dai, Nature (London) **453**, 899 (2008).
[10] Y. Chen, J. W. Lynn, J. Li, G. Li, G. F. Chen, J. L. Luo, N. L. Wang, P. Dai, C. de la Cruz, and H. A. Mook, Phys. Rev. B **78**, 064515 (2008).
[11] A. I. Goldman, D. N. Argyriou, B. Ouladdiaf, T. Chatterji, A. Kreyssig, S. Nandi, N. Ni, S. L. Bud'ko, P. C. Canfield, and R. J. McQueeney, Phys. Rev. B **78**, 100506(R) (2008).
[12] D. J. Singh and M.-H. Du, Phys. Rev. Lett. **100**, 237003 (2008).
[13] S. Lebegue, Phys. Rev. B **75**, 035110 (2007).
[14] G. Xu, W. Ming, Y. Yao, X. Dai, S.-C. Zhang, and Z. Fang, EPL **82**, 67002 (2008).
[15] C. Cao, P. J. Hirschfeld, and H.-P. Cheng, Phys. Rev. B **77**, 220506(R) (2008).
[16] H.-J. Zhang, G. Xu, X. Dai, and Z. Fang, Chin. Phys. Lett. **26**, 017401 (2009).
[17] M. Daghofer, A. Moreo, J. A. Riera, E. Arrigoni, D. J. Scalapino, and E. Dagotto, Phys. Rev. Lett. **101**, 237004 (2008).
[18] Q. Si and E. Abrahams, Phys. Rev. Lett. **101**, 076401 (2008).
[19] J. Jaroszynski, S. C. Riggs, F. Hunte, A. Gurevich, D. C. Larbalestier, G. S. Boebinger, F. F. Balakirev, A. Migliori, Z. A. Ren, W. Lu, J. Yang, X. L. Shen, X. L. Dong, Z. X. Zhao, R. Jin, A. S. Sefat, M. A. McGuire, B. C. Sales, D. K. Christen, and D. Mandrus, Phys. Rev. B **78**, 064511 (2008).
[20] M. M. Qazilbash, J. J. Hamlin, R. E. Baumbach, M. B. Maple, and D. N. Basov, arXiv:0808.3748 (unpublished).
[21] Y. Ishida, T. Shimojima, K. Ishizaka, T. Kiss, M. Okawa, T. Togashi, S. Watanabe, X. Y. Wang, C. T. Chen, Y. Kamihara, M. Hirano, H. Hosono, and S. Shin, Phys. Rev. B **79**, 060503(R) (2009).
[22] T. Sato, S. Souma, K. Nakayama, K. Terashima, K. Sugawara, T. Takahashi, Y. Kamihara, M. Hirano, and H. Hosono, J. Phys. Soc. Jpn. **77**, 063708 (2008).
[23] H.-Y. Liu, X.-W. Jia, W.-T. Zhang, L. Zhao, J.-Q. Meng, G.-D. Liu, X.-L. Dong, G. Wu, R.-H. Liu, X.-H. Chen, Z.-A. Ren, W. Yi, G.-C. Che, G.-F. Chen, N.-L. Wang, G.-L. Wang, Y. Zhou, Y. Zhu, X.-Y. Wang, Z.-X. Zhao, Z.-Y. Xu, C.-T. Chen, and X.-J. Zhou, Chin. Phys. Lett. **25**, 3761 (2008).
[24] L. Zhao, H.-Y. Liu, W.-T. Zhang, J.-Q. Meng, X.-W. Jia, G.-D. Liu, X.-L. Dong, G.-F. Chen, J.-L. Luo, N.-L. Wang, W. Lu, G.-L. Wang, Y. Zhou, Y. Zhu, X.-Y. Wang, Z.-Y. Xu, C.-T. Chen, and X.-J. Zhou, Chin. Phys. Lett. **25**, 4402 (2008).
[25] We note that it is still under debate in *ab initio* calculations whether a pseudogap exists in the undoped iron pnictide. Early DFT result in Ref. 12 suggests that the DOS at the chemical potential is located at the edge of a sharp peak; later calculations in the $(\pi,0)$ antiferromagnetic state reveal a pseudogap in the DOS near the Fermi level [see, for instance, Ref. 77; J. Dong, H. J. Zhang, G. Xu, Z. Li, G. Li, W. Z. Hu, D. Wu, G. F. Chen, X. Dai, J. L. Luo, Z. Fang, and N. L. Wang, Europhys. Lett. **83**, 27006 (2008); Z. P. Yin, S. Lebègue, M. J. Han, B. P. Neal, S. Y. Savrasov, and W. E. Pickett, Phys. Rev. Lett. **101**, 047001 (2008)]. However, a recent LDA+DMFT(QMC) calculation [A. O. Shorikov, M. A. Korotin, S. V. Streltsov, D. M. Korotin, and V. I. Anisimov, arXiv:0804.3283 (unpublished)] finds a peak at the Fermi level of DOS, although the system is in the intermediate correlation strength regime. Considering the discrepancies in theories, here we will rely on the experimental findings in Refs. 21–24.
[26] K. Kuroki, S. Onari, R. Arita, H. Usui, Y. Tanaka, H. Kontani, and H. Aoki, Phys. Rev. Lett. **101**, 087004 (2008).
[27] I. I. Mazin, D. J. Singh, M. D. Johannes, and M. H. Du, Phys. Rev. Lett. **101**, 057003 (2008).
[28] X. Dai, Z. Fang, Y. Zhou, and F.-C. Zhang, Phys. Rev. Lett. **101**, 057008 (2008).
[29] Q. Han, Y. Chen, and Z. D. Wang, EPL **82**, 37007 (2008).
[30] M. M. Korshunov and I. Eremin, Phys. Rev. B **78**, 140509(R) (2008).
[31] G. Baskaran, J. Phys. Soc. Jpn. **77**, 113713 (2008).
[32] Z.-J. Yao, J.-X. Li, and Z. D. Wang, New J. Phys. **11**, 025009 (2009).
[33] C. Xu, M. Müller, and S. Sachdev, Phys. Rev. B **78**, 020501(R) (2008).
[34] P. A. Lee and X.-G. Wen, arXiv:0804.1739 (unpublished).
[35] T. Yildirim, Phys. Rev. Lett. **101**, 057010 (2008).
[36] S. Raghu, X.-L. Qi, C.-X. Liu, D. J. Scalapino, and S.-C. Zhang, Phys. Rev. B **77**, 220503(R) (2008).
[37] K. Seo, B. A. Bernevig, and J. Hu, Phys. Rev. Lett. **101**, 206404

(2008).
[38] Y. Zhou, W.-Q. Chen, and F.-C. Zhang, Phys. Rev. B **78**, 064514 (2008).
[39] J. Lorenzana, G. Seibold, C. Ortix, and M. Grilli, Phys. Rev. Lett. **101**, 186402 (2008).
[40] R. Sknepnek, G. Samolyuk, Y. bin Lee, B. N. Harmon, and J. Schmalian, Phys. Rev. B **79**, 054511 (2009).
[41] M. M. Parish, J. Hu, and B. A. Bernevig, Phys. Rev. B **78**, 144514 (2008).
[42] H.-Y. Choi and Y. Bang, arXiv:0807.4604 (unpublished).
[43] Z.-H. Wang, H. Tang, Z. Fang, and X. Dai, arXiv:0805.0736 (unpublished).
[44] S. Yang, W.-L. You, S.-J. Gu, and H.-Q. Lin, arXiv:0807.0587, Chin. Phys. B (to be published).
[45] J. Shi, arXiv:0806.0259 (unpublished).
[46] W.-L. You, S.-J. Gu, G.-S. Tian, and H.-Q. Lin, Phys. Rev. B **79**, 014508 (2009).
[47] M. J. Calderon, B. Valenzuela, and E. Bascones, New J. Phys. **11**, 013051 (2009).
[48] K. Hashimoto, T. Shibauchi, T. Kato, K. Ikada, R. Okazaki, H. Shishido, M. Ishikado, H. Kito, A. Iyo, H. Eisaki, S. Shamoto, and Y. Matsuda, Phys. Rev. Lett. **102**, 017002 (2009).
[49] T. Kondo, A. F. Santander-Syro, O. Copie, C. Liu, M. E. Tillman, E. D. Mun, J. Schmalian, S. L. Bud'ko, M. A. Tanatar, P. C. Canfield, and A. Kaminski, Phys. Rev. Lett. **101**, 147003 (2008).
[50] H. Ding, P. Richard, K. Nakayama, K. Sugawara, T. Arakane, Y. Sekiba, A. Takayama, S. Souma, T. Sato, T. Takahashi, Z. Wang, X. Dai, Z. Fang, G. F. Chen, J. L. Luo, and N. L. Wang, EPL **83**, 47001 (2008).
[51] C. Martin, R. T. Gordon, M. A. Tanatar, M. D. Vannette, M. E. Tillman, E. D. Mun, P. C. Canfield, V. G. Kogan, G. D. Samolyuk, J. Schmalian, and R. Prozorov, arXiv:0807.0876 (unpublished).
[52] T. Y. Chen, Z. Tesanovic, R. H. Liu, X. H. Chen, and C. L. Chien, Nature (London) **453**, 1224 (2008).
[53] D. Parker, O. V. Dolgov, M. M. Korshunov, A. A. Golubov, and I. I. Mazin, Phys. Rev. B **78**, 134524 (2008).
[54] V. B. Zabolotnyy, D. S. Inosov, D. V. Evtushinsky, A. Koitzsch, A. A. Kordyuk, J. T. Park, D. Haug, V. Hinkov, A. V. Boris, D. L. Sun, G. L. Sun, C. T. Lin, B. Keimer, M. Knupfer, B. Buechner, A. Varykhalov, R. Follath, and S. V. Borisenko, Nature **457**, 569 (2009).
[55] E. Dagotto, Rev. Mod. Phys. **66**, 763 (1994).
[56] M. Potthoff, M. Aichhorn, and C. Dahnken, Phys. Rev. Lett. **91**, 206402 (2003).
[57] M. Potthoff, Eur. Phys. J. B **36**, 335 (2003).
[58] J. P. Van Dyke and G. A. Samara, Phys. Rev. B **11**, 4935 (1975).
[59] B. I. Min, H. J. F. Jansen, and A. J. Freeman, Phys. Rev. B **33**, 6383 (1986).
[60] D. Duan, Y. Liu, Y. Ma, Z. Liu, T. Cui, B. Liu, and G. Zou, Phys. Rev. B **76**, 104113 (2007).
[61] D. Duffy and A. Moreo, Phys. Rev. B **55**, R676 (1997).
[62] L. M. Sander, H. B. Shore, and J. H. Rose, Phys. Rev. B **24**, 4879 (1981).
[63] J. Callaway and D. G. Kanhere, Phys. Rev. B **49**, 12823 (1994).
[64] A. Camjayi, R. Chitra, and M. J. Rozenberg, Phys. Rev. B **73**, 041103(R) (2006), and references therein.
[65] S. Miyasaka, H. Takagi, Y. Sekine, H. Takahashi, N. Môri, and R. J. Cava, J. Phys. Soc. Jpn. **69**, 3166 (2000), and references therein.
[66] P. G. Niklowitz, P. L. Alireza, M. J. Steiner, G. G. Lonzarich, D. Braithwaite, G. Knebel, J. Flouquet, and J. A. Wilson, Phys. Rev. B **77**, 115135 (2008).
[67] Y. Moritomo, T. Akimoto, A. Nakamura, K. Ohoyama, and M. Ohashi, Phys. Rev. B **58**, 5544 (1998).
[68] G. Cao, S. C. McCall, J. E. Crow, and R. P. Guertin, Phys. Rev. B **56**, 5387 (1997).
[69] T. Otsuka, A. Kobayashi, Y. Miyamoto, J. Kiuchi, S. Nakamura, N. Wada, E. Fujiwara, H. Fujiwara, and H. Kobayashi, J. Solid State Chem. **159**, 407 (2001), and references therein.
[70] T. Otsuka, H. Cui, H. Fujiwara, H. Kobayashi, E. Fujiwara, and A. Kobayashi, J. Mater. Chem. **14**, 1682 (2004), and references therein.
[71] W. Bao, C. Broholm, S. A. Carter, T. F. Rosenbaum, G. Aeppli, S. F. Trevino, P. Metcalf, J. M. Honig, and J. Spalek, Phys. Rev. Lett. **71**, 766 (1993).
[72] J. C. Slater and G. F. Koster, Phys. Rev. **94**, 1498 (1954).
[73] A. Moreo, M. Daghofer, J. A. Riera, and E. Dagotto, arXiv:0901.3544 (unpublished).
[74] E. Dagotto, T. Hotta, and A. Moreo, Phys. Rep. **344**, 1 (2001).
[75] T. Nomura and K. Yamada, J. Phys. Soc. Jpn. **69**, 1856 (2000).
[76] By symmetry consideration, the state ordered at $(\pi,0)$ will give exactly the same result with interchange in the *xz* and *yz* orbitals.
[77] K. Haule, J. H. Shim, and G. Kotliar, Phys. Rev. Lett. **100**, 226402 (2008).
[78] S. Haas, A. Moreo, and E. Dagotto, Phys. Rev. Lett. **74**, 4281 (1995), and references therein.
[79] B. O. Wells, Z. X. Shen, A. Matsuura, D. M. King, M. A. Kastner, M. Greven, and R. J. Birgeneau, Phys. Rev. Lett. **74**, 964 (1995).
[80] D. H. Lu, M. Yi, S. K. Mo, A. S. Erickson, J. Analytis, J. H. Chu, D. J. Singh, Z. Hussain, T. H. Geballe, I. R. Fisher, and Z. X. Shen, Nature **455**, 81 (2008).
[81] J. G. Analytis, J.-H. Chu, A. S. Erickson, C. Kucharczyk, A. Serafin, A. Carrington, C. Cox, S. M. Kauzlarich, H. Hope, and I. R. Fisher, arXiv:0810.5368 (unpublished).
[82] M. S. Laad, L. Craco, S. Leoni, and H. Rosner, Phys. Rev. B **79**, 024515 (2009).
[83] J. Dai, Q. Si, J. Zhu, and E. Abrahams, arXiv:0808.0305, Proc. Natl. Acad. Sci. (USA) (to be published).